Planetary and Space Science 85 (2013) 232–242

Contents lists available at ScienceDirect

Planetary and Space Science

journal homepage: www.elsevier.com/locate/pss

Lunar energetic neutral atom (ENA) spectra measured by the interstellar boundary explorer (IBEX)

F. Allegrini [a,b,*], M.A. Dayeh [a], M.I. Desai [a,b], H.O. Funsten [c], S.A. Fuselier [a], P.H. Janzen [d], D.J. McComas [a,b], E. Möbius [e], D.B. Reisenfeld [d], D.F. Rodríguez M. [f], N. Schwadron [e], P. Wurz [f]

[a] Southwest Research Institute, P.O. Drawer 28510, San Antonio, TX 78228, USA
[b] University of Texas at San Antonio, Physics and Astronomy Department, San Antonio, TX 78249, USA
[c] Los Alamos National Laboratory, Los Alamos, Bikini Atoll Rd., SM 30, NM 87545, USA
[d] University of Montana, 32 Campus Drive, Missoula, MT, USA
[e] University of New Hampshire, Space Science Center, Physics and Astronomy Department, Morse Hall Room 407, Durham, NH 03824, USA
[f] Physikalisches Institut, Universität Bern, Sidlerstrasse 5, 3012 Bern, Switzerland

ARTICLE INFO

Article history:
Received 11 March 2013
Received in revised form
6 May 2013
Accepted 17 June 2013
Available online 24 June 2013

Keywords:
Energetic neutral atoms
ENA Moon albedo
Solar wind
IBEX

ABSTRACT

The solar wind continuously flows out from the Sun, filling interplanetary space and directly interacting with the surfaces of small planetary bodies and other objects throughout the solar system. A significant fraction of these ions backscatter from the surface as energetic neutral atoms (ENAs). The first observations of these ENA emissions from the Moon were recently reported from the Interstellar Boundary Explorer (IBEX). These observations yielded a lunar ENA albedo of ~10% and showed that the Moon reflects ~150 metric tons of neutral hydrogen per year. More recently, a survey of the first 2.5 years of IBEX observations of lunar ENAs was conducted for times when the Moon was in the solar wind. Here, we present the first IBEX ENA observations when the Moon is inside the terrestrial magnetosheath and compare them with observations when the Moon is in the solar wind. Our analysis shows that: (1) the ENA intensities are on average higher when the Moon is in the magnetosheath, (2) the energy spectra are similar above ~0.6* solar wind energy but below there are large differences of the order of a factor of 10, (3) the energy spectra resemble a power law with a "hump" at ~0.6 * solar wind energy, and (4) this "hump" is broader when the Moon is in the magnetosheath. We explore potential scenarios to explain the differences, namely the effects of the topography of the lunar surface and the consequences of a very different Mach number in the solar wind versus in the magnetosheath.

1. Introduction

The Interstellar Boundary Explorer (IBEX) (McComas et al., 2009a) was launched on Oct. 19, 2008 and has been delivering a number of exciting results ever since. Aside from its goals to study the global interactions between the heliosphere and the local interstellar medium using energetic neutral atom (ENA) imaging, IBEX also observes nearby objects (McComas et al., 2011a), namely the terrestrial magnetosphere (e.g., McComas et al., 2011b, 2012; Petrinec et al., 2011; Fuselier et al., 2010) and the Moon (McComas et al., 2009; Rodriguez et al., 2012; Funsten et al., 2013).

IBEX has two single-pixel, high-sensitivity ENA imagers (or sensors), IBEX-Lo and IBEX-Hi, that have overlapping energy ranges from ~0.01 to 2 keV and from ~0.3 and 6 keV, respectively. Both sensors use a similar detection technique: a collimator to define the field-of-view (FOV) and repel charged particles, a charge conversion system to convert the ENAs into charged particles, an energy analyzer to filter the ionized ENAs by energy and to block UV radiation, and a coincidence detection section. For the charge conversion system, IBEX-Lo utilizes a very smooth conversion surface (e.g., Scheer et al., 2006), whereas IBEX-Hi utilizes an ultra-thin carbon foil (e.g., Funsten et al., 1993; McComas et al., 2004). Their FOVs are similar (~$7^\circ \times 7^\circ$ FWHM) and their look directions are on opposite sides of the spacecraft, perpendicular to the spin axis, such that they both sample the same swath in the sky over a full spacecraft spin. Both IBEX sensors resolve energy ($\Delta E/E$~0.7 FHWM in eight steps for IBEX-Lo and ~0.5 to 0.7 FHWM in six steps for IBEX-Hi). More detailed information on these sensors can be found in the respective instrument papers (Fuselier et al., 2009; Funsten et al., 2009). IBEX also has a background monitor (IBaM for IBEX Background Monitor) (Allegrini et al., 2009) that is used to infer the ion background environment and to identify time intervals when the

* Corresponding author at: Southwest Research Institute, P.O. Drawer 28510, San Antonio, TX 78228, USA. Tel.: +1 210 522 6029; fax: +1 210 520 9935.
E-mail address: fallegrini@swri.edu (F. Allegrini).

0032-0633/$ - see front matter © 2013 Elsevier Ltd. All rights reserved.
http://dx.doi.org/10.1016/j.pss.2013.06.014

background signal is above an energy and flux threshold. The IBaM makes an integral measurement of protons intensities above ~14 keV.

The first report of ENAs from the Moon (McComas et al., 2009b) used IBEX-Hi observations taken in December 2008, during the first IBEX-Hi commissioning orbit. This study established that the ENAs were solar wind backscattered from and neutralized by the surface of the Moon. The reflected portion, or ENA albedo, was estimated to be ~10% based on this one observation of the Moon.

Soon after, Wieser et al. (2009) reported the first observations of ENAs measurements from the Chandrayaan-1 Energetic Neutral Atom (CENA) (Kazama et al., 2007) sensor part of the SARA instrument (Bhardwaj et al., 2005; Barabash et al., 2009). CENA is based on the conversion surface technique, similar to IBEX-Lo (Wurz, 2000). Chandrayaan-1 was in a polar orbit around the Moon at 100 km altitude. CENA measured an ENA albedo of ~16–20% in the energy range ~40 to 650 eV. Using a large collection of CENA measurements, Schaufelberger et al. (2011) determined a scattering function of lunar ENAs over this energy range. Contrary to what is observed with atomically smooth surfaces for which forward scattering is favored, the results showed that backscattering was favored in the case of the lunar regolith, probably because of the large porosity. Using the full energy range of CENA (10–3300 eV), Futaana et al. (2012) reported ENA energy spectra. They found that the best fit to their spectra was with Maxwell–Boltzmann distributions and with the only correlation between the fit parameters and the upstream solar wind parameters was the solar wind speed with the characteristic energy of the ENAs.

Recently, Rodríguez et al. (2012) reported IBEX-Lo observations of lunar ENAs. They derived an ENA albedo of ~0.09. Building on Schaufelberger et al. (2011) scattering function, Saul et al. (2013) recalculated the ENA albedo from the IBEX-Lo measurements and found an albedo about 25% higher, i.e., 0.11.

Since the first report of lunar ENA measured by IBEX-Hi, Funsten et al. (2013) analyzed many more observations when the Moon was in the solar wind. They derived key properties of the lunar ENAs, and in particular found that the albedo varies from about 0.08 to 0.20 depending on solar wind speed. It is lowest for the highest solar wind speed and is empirically fitted with the function $R_N = 1/(2.3+6.3\ E_{SW}$ [keV]). They also found strong evidence of an ENA spectral distribution at energies greater than ~250 eV that decreases linearly with increasing energy up to the solar wind energy.

There are times, however, when the Moon is in the magnetosheath as it transits IBEX's FOV. In the magnetosheath, the plasma incident on the Moon is different from the solar wind input of previous studies. Specifically, the solar wind is slowed, compressed and heated at the bow shock, and flow is diverted around the magnetosphere. This contrasts to direct exposure to the solar wind, which is generally beam-like. Some parameters, such as the Mach number, are changed in the magnetosheath and that may result in a different reflection coefficient because more of the surface visible from IBEX could be exposed to the solar wind.

In this study, we combine for the first time IBEX-Lo and -Hi observations of lunar ENAs to create spectra over the broad energy range from ~14 eV to ~4.1 keV for the viewings when the Moon is in the magnetosheath or in the solar wind. We then compare these spectra and evaluate the differences between observations when the Moon is in the magnetosheath and the solar wind.

2. Data selection

We examine all data intervals, when the Moon is either in the solar wind or in the magnetosheath, in which IBEX observes statistically significant counts in both IBEX-Lo and -Hi. Specifically, the number of counts attributed to lunar ENAs is larger than one standard deviation in more than one energy step (total of eight steps for IBEX-Lo and six for IBEX-Hi). The driver for good intervals is usually the IBEX-Lo sensor because IBEX-Hi is more sensitive than IBEX-Lo. We end up with a total of nine viewings from orbit 11 (end of December 2008) up to orbit 139 (mid September 2011), four of them being when the Moon is in the solar wind, and five when the Moon is in the magnetosheath. Table 1 lists the intervals and Fig. 1 shows two examples of the configuration when (a) the Moon is in the solar wind (orbit 58, December 2009) and (b) when the Moon is in the magnetosheath (orbit 136a, August 2011). We use a model of the magnetosphere to determine if the Moon is in the magnetosheath (more details are given below).

Table 1
Time intervals in UT of the lunar viewings. The abbreviations of the location are SW for solar wind and MS for magnetosheath.

orbit	Date start yyyy/mm/dd	Time start hh:mm:ss	Date stop yyyy/mm/dd	Time stop hh:mm:ss	Location
29	2009/05/16	13:43:28	2009/05/17	02:01:36	SW
43	2009/08/30	21:46:51	2009/08/31	10:01:22	MS
44	2009/09/07	20:21:02	2009/09/08	23:52:50	MS
58	2009/12/21	15:32:16	2009/12/22	03:50:24	SW
72	2010/04/08	11:54:40	2010/04/08	22:41:04	SW
126	2011/05/24	09:38:08	2011/05/24	17:18:56	SW
136a	2011/08/17	00:01:50	2011/08/17	13:47:59	MS
138b	2011/09/07	11:40:15	2011/09/07	22:22:55	MS
139b	2011/09/15	03:05:15	2011/09/16	15:54:08	MS

Figs. 2 and 3 show examples of data for the orbit arc 136a for IBEX-Lo and -Hi, respectively. The counts per time bin (923 s bin for IBEX-Lo and 919 s bin for IBEX-Hi) are color-coded and plotted in angle from north ecliptic pole (NEP) versus time for each energy step on the right-hand side. The orange vertical bars represent the time intervals of the lunar viewing. The top panel displays the background monitor counts in the same representation for the full angle range. The rectangle corresponds to the range of angles covered in the lower panels. Times when the background monitor rates are above a defined threshold or when the Moon is outside the magnetosheath (for a magnetosheath interval) are disregarded as indicated by the gray shading. The counts are then integrated over the time interval and plotted as a function of angle from NEP on the right-hand side.

IBEX's FOV is ~$7^\circ \times 7^\circ$ FWHM with a roughly triangular transmission function. IBEX data are binned in histograms of sixty six-degree bins. From IBEX's point-of-view, the Moon's full disk in the FOV ranges from ~0.55° to 2.1° for the selected viewings. Therefore, the lunar ENA counts appear at most within three consecutive angle bins.

To extract the lunar counts from a residual background (that can be partly attributed to heliospheric signal) we fit an empirical second-degree polynomial (dark blue curve) to the pixels (green dots) on each side of the peaks (red dots) and subtract it from the counts in the peaks. The total lunar ENA counts with background subtracted are indicated as well as the one-sigma uncertainty for each energy step.

3. Results

3.1. Lunar ENA energy spectra

The lunar ENAs counts for IBEX-Lo and -Hi are then converted into rates and subsequently into fluxes using the respective geometric factors for hydrogen (see Table 2). The fluxes for IBEX-Lo are

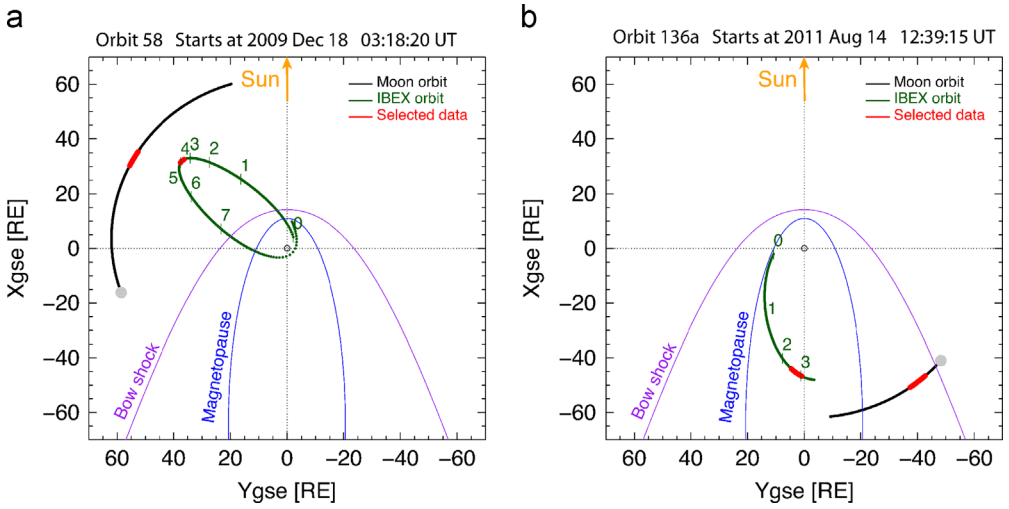

Fig. 1. Examples of observations when (a) the Moon is in the solar wind and (b) when the Moon is in the magnetosheath. IBEX's orbital path is shown in green and that of the Moon (gray point), for the duration of IBEX's orbit, is shown in black. The locations of IBEX and the Moon for the selected viewing intervals are shown in red on their respective orbit paths.

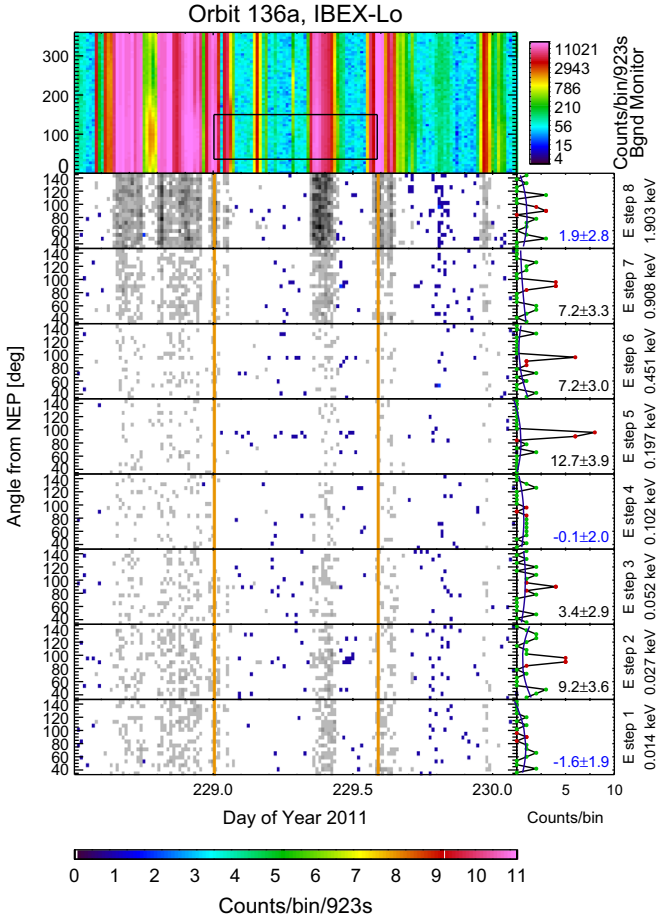

Fig. 2. Example of data from IBEX-Lo for the viewing in orbit arc 136a (mid Aug. 2011). The bottom panels show the counts per bin plotted in angle from north ecliptic pole (NEP) versus time for each energy step. Times when the background monitor (top panel) measures a signal above a defined threshold rate or when the Moon is outside the magnetosheath (for a magnetosheath interval) are disregarded (gray shading). The counts are integrated over the time interval delimited by the orange vertical lines. A second background subtraction uses the pixels around the peaks. The lunar ENA counts are clearly visible for energy steps 2, 3, 5, 6, and 7 on the right panels.

calculated using

$$F_{\mathrm{Lo},i} = C_{\mathrm{Lo},i}/(\Delta T_{\mathrm{Lo}} * 8 * G_{\mathrm{Lo},i}) \quad (1)$$

where $C_{\mathrm{Lo},i}$ are the total lunar ENA counts at energy step "i", ΔT_{Lo} is the integration time of the viewing for IBEX-Lo, $G_{\mathrm{Lo},i}$ is the geometric factor at energy step "i", and the factor of 8 accounts for the eight energy steps of an IBEX-Lo measurement cycle. Similarly, for IBEX-Hi we have:

$$F_{\mathrm{Hi},i} = C_{\mathrm{Hi},i}/(\Delta T_{\mathrm{Hi}} * 6 * G_{\mathrm{Hi},i}) \quad (2)$$

where the "Lo" subscript has been replaced with "Hi" and the factor 8 by a factor 6 because IBEX-Hi steps over six energy steps.

As mentioned in the introduction, the charge conversion system in the IBEX-Lo sensor is a specialized surface (Wurz et al., 2006). Some of the neutral atoms sputter residual material (e.g., water) present on the surface. Thus, an ENA at a given energy can produce sputtered components at a somewhat lower energy. The sputtered ion may have the right energy to pass through the energy analyzer and be detected in the detector section, thus masquerading as a legitimate count. The sputtered contributions to the signal have been calibrated before flight and are summarized in the form of Table 3 (adapted from Rodríguez et al. (2012)). We use this information to determine the corrections to apply to the fluxes calculated with equation (1).

We proceed as follows. We start with the last column of the table "E step 8," for which the flux is not corrected. We assume that the sputtering contributions from higher energies than energy step 8 are negligible because the flux at higher energies is small in comparison to that in energy step 8 or below due to the steep power law of the energy spectra as will be shown below. Then, we subtract 0.304 times the flux in step 8 to the flux in step 7. The result is the corrected flux in step 7. To calculate the corrected flux in step 6 we subtract 0.107 times the flux in step 8 and 0.334 times the corrected flux in step 7—that we just calculated above—to the flux in step 6. The value we obtain is the corrected flux in step 6. The method continues until we calculate the corrected flux in energy step 1.

The sputter correction to the measured ENA flux values is relatively modest. For example, the fluxes are reduced by ~25% in average for all energy steps and viewings. The minimum correction is ~5% for energy step 7 and the maximum is ~45% for energy step 5. For energy step 5 and below, the average correction reduces

the flux by ~35%. These values are comparable to, though slightly higher than, those calculated in Fuselier et al. (2012) where they corrected fluxes for heliopsheric ENAs.

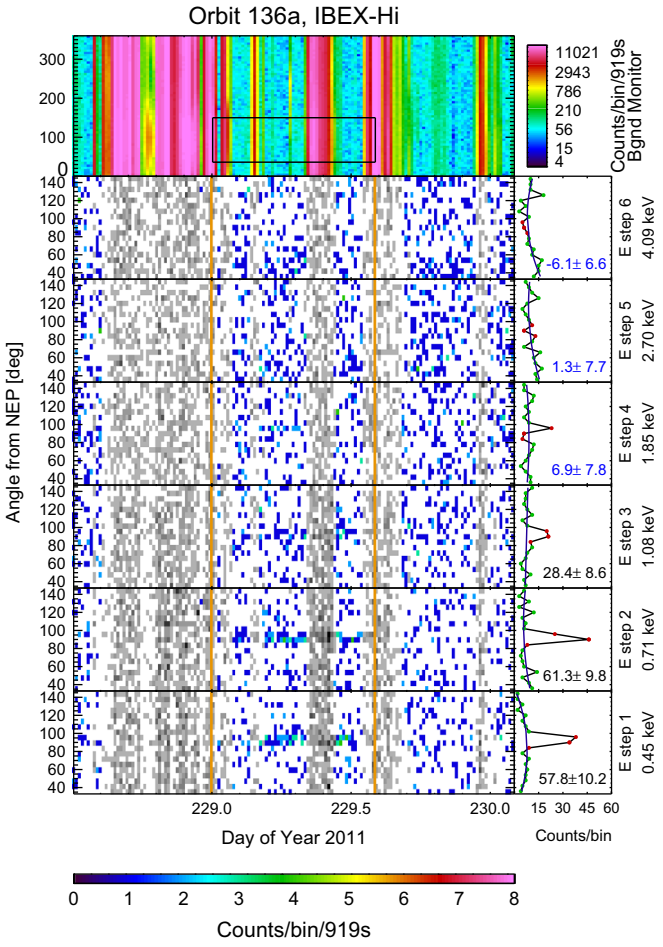

Fig. 3. Same as Fig. 2 for IBEX-Hi data.

The final energy spectra are shown in Fig. 4. The data points are in green for IBEX-Hi and in orange for IBEX-Lo. Note that since IBEX-Lo and -Hi are co-located, there is no correction required to compare the fluxes on the same scale. There is excellent agreement between the average flux values in the overlapping energy range of the IBEX-Lo and -Hi sensors. Because they use different detection techniques to register the ENAs, this makes for an independent verification of the fluxes. The lighter colors symbols are used when one standard deviation is larger than the flux value. The dotted curves represent the one-count limit for the entire viewing interval. Two data points (in Orbit 126 and 138b) fall below this one-count limit because of the background subtraction and the sputter correction. Even though they have a large relative uncertainty, these points are not removed from the analysis below unless stated. To make sure that we did not include a bias one way or another, we verified that the end results did not change much whether they are included or not.

The average energy spectra in physical units have similar shapes in that they are fairly flat below some energy and decrease with energy as power laws for higher energies. This is very similar to what is expected for backscattered hydrogen from a regolith-like material when simulated with the Transport of Ion through Matter (TRIM) software (see Funsten et al., 2013).

To compare the energy spectra across different observations, we need to apply several normalization factors: (1) the IBEX-Moon distance, (2) the Moon location in IBEX's FOV, (3) the solar wind speed, (4) the solar wind flux, and (5) the solar wind flow direction. We describe below how we apply these normalizations in more details.

From IBEX's point-of-view, the Moon can be approximated as a point source. We assume that the ENA flux decreases as $1/R^2$, where R is the IBEX-Moon distance. The lunar observations span a few hours, typically around 12 h except for orbit 44 (~28 h) and orbit 139b (~79 h), where the Moon and IBEX happened to be moving together in a similar way in their orbits. The IBEX-Moon distance over these relatively short periods of time does not vary much and we use the average distance and multiply the fluxes by R^2 for our correction.

As mentioned earlier, the IBEX collimator has a roughly triangular angular response function. When the Moon passes across the FOV, the transmission varies from zero to a maximum and back to zero as illustrated in Fig. 5(a). But sometimes, such as

Table 2
IBEX-Lo and -Hi geometric factors for hydrogen.

	E step	1	2	3	4	5	6	7	8
IBEX-Lo	E_0 [keV]	0.014	0.027	0.052	0.102	0.197	0.451	0.908	1.903
	G_{Lo} 1E−5 * [cm^2 sr eV/eV]	0.729	1.41	2.17	2.43	2.41	2.82	5.23	7.41
IBEX-Hi	E_0 [keV]	0.45	0.71	1.08	1.85	2.70	4.09		
	G_{Hi} 1E−3 * [cm^2 sr eV/eV]	0.13	0.41	0.75	1.3	2.4	4.5		

Table 3
Relative flux correction factors due to sputtering on the conversion surface in IBEX-Lo (adapted from Rodríguez et al., 2012). See text for the method.

	E step 1	E step 2	E step 3	E step 4	E step 5	E step 6	E step 7	E step 8
Relative flux contributions to lower energy steps	1	0	0	0	0	0	0	0
	0.523	1	0	0	0	0	0	0
	0.0859	0.4[a]	1	0	0	0	0	0
	0.0225	0.05[a]	0.28	1	0	0	0	0
	0.0213	0.03[a]	0.0552	0.3[a]	1	0	0	0
	0.0216	0.03[a]	0.0399	0.05[a]	0.3795	1	0	0
	0.0235	0.0209	0.0314	0.0549	0.107	0.334	1	0
	0.0216	0.00752	0.0254	0.0451	0.0541	0.107	0.304	1

[a] These values are interpolated.

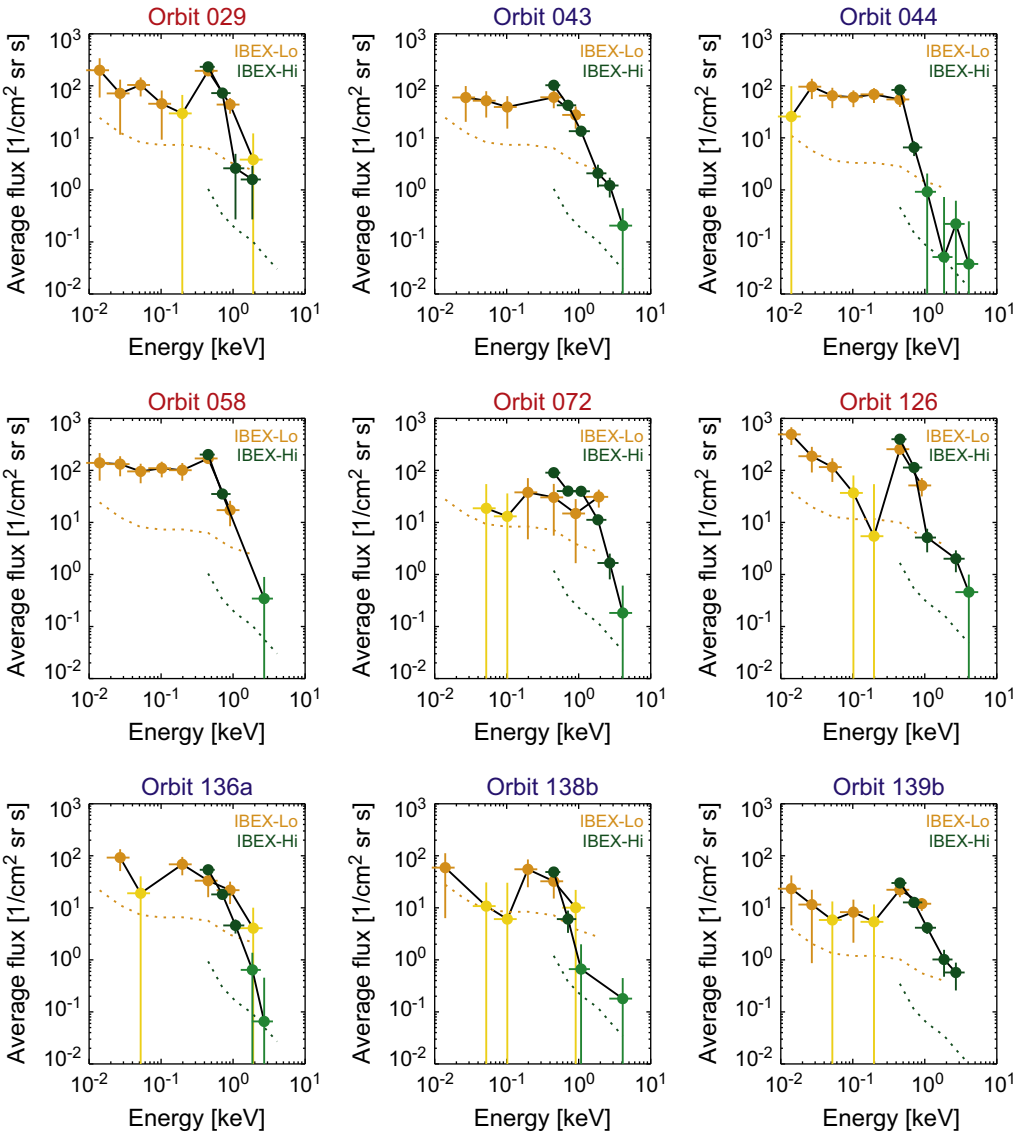

Fig. 4. Calculated ENA flux at each energy passband versus the nominal passband energy for the nine lunar viewings. The lighter color symbols identify when the standard deviation is larger than the flux value. The color of the title refers to solar wind interval in red and magnetosheath interval in blue. The dotted curves represent the one-count level.

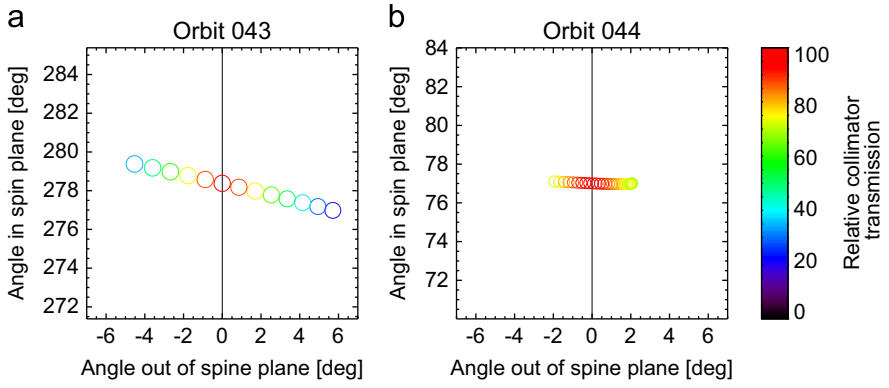

Fig. 5. Examples of the passage of the Moon in IBEX's FOV for orbit 43 (a) and 44 (b). The circles represent the Moon imb and they are plotted in 1 h intervals. The color of the circle corresponds to the relative transmission of the collimator using a rainbow color coding (red = maximum transmission).

shown in Fig. 5(b), the combination of the motion of IBEX and that of the Moon makes the Moon spend more time in the center of the FOV where the collimator transmission is higher. To account for these differences we calculate the average transmission for each viewing interval and divide the fluxes by these averages.

The energy distribution of the reflected and neutralized solar wind depends on the impinging solar wind energy (Wieser et al., 2009; Rodríguez et al., 2012; Futaana et al., 2012; Funsten et al., 2013). Since IBEX resolves the energy of the ENA, we have to account for these differences in the distributions and we

normalize the energy to the solar wind energy. The solar wind parameters are downloaded from the OMNIWeb Plus website (http://omniweb.gsfc.nasa.gov/hw.html). To estimate the magnetosheath plasma parameters, we asked the Community Coordinated Modeling Center at Goddard Space Flight Center (http://ccmc.gsfc.nasa.gov/) to run a magnetosphere model (BATSRUS) for the intervals in orbits 43, 44, 136a, 138b, and 139b. From the model output we calculated the average bulk speed (assuming protons) of the magnetosheath flow. We divide the IBEX energy per charge by the derived energy per charge.

The ENA flux from the Moon is directly proportional to the input plasma flux, as demonstrated by McComas et al. (2009b). Therefore, we normalize the measured ENA fluxes with the average solar wind or magnetosheath flux (speed times density) obtained from OMNIWeb Plus or the simulations above.

The last normalization factor has to do with the area of the Moon illuminated by the solar wind that is visible from IBEX. The solar wind propagates roughly radially from the Sun. Because of the Earth's motion around the Sun, the solar wind direction is slightly aberrated. Therefore, the portion of the lunar disk that is in the solar wind and at the same time visible from IBEX depends on the aberration angle. The aberration angle is calculated using the solar wind velocity components which are obtained either from OMNIWeb for the solar wind intervals or the BASTRUS model for the magnetosheath intervals. The aberration angle ranges (in absolute value) from 2.9° to 4.9° when the Moon is in the solar wind and from 8.9° to 12.7° when the Moon is in the magnetosheath. We then calculate the portion of the disk that is illuminated as viewed by IBEX and divide the ENA flux by this number.

We now normalize the energy spectra from Fig. 4 and compare them in Fig. 6 by plotting the normalized differential energy fluxes as a function of energy normalized to solar wind energy. Fig. 6(a) shows the spectra when the Moon is in the solar wind and Fig. 6(b) shows the same when the Moon is in the magnetosheath.

When the Moon is in the solar wind, the spectra all show the similar intensities except for the viewing during orbit 72 which has about a factor of ten less intensity at ~0.6*solar wind energy. The largest differences between the energy spectra are seen at energies around 0.1–0.2*solar wind energy. All the spectra show a "hump" around 0.6* solar wind energy. The solar wind protons are not mono-energetic and their energy distribution extends beyond $E/E_{SW}=1$. Moreover, the IBEX-Hi energy bins are about ~0.5 to 0.7 (ΔE/E at FWHM). It is therefore not surprising to see ENAs above one solar wind energy.

When the Moon is in the magnetosheath, the spectra also have more or less the same characteristic shape with a "hump" around 0.6–0.8 times the solar wind energy. There seem to be more variations from spectrum to spectrum compared to the solar wind intervals. The spectra for the viewings in orbits 44 and 136a are significantly higher than the others. The viewings in orbit 43 and 139b are remarkably similar.

While the spectra above ~0.6* solar wind energy all have similar shape for all intervals, there are noticeable differences at energies below the "hump": the spectra from the magnetosheath intervals appear harder (flatter) than the spectra in the solar wind intervals. Moreover, the "hump" is a lot broader for the magnetosheath than for the solar wind intervals.

In Fig. 7 we compare the solar wind intervals (in blue) with the magnetosheath intervals (in red). It is clear that at least two viewings in the magnetosheath have higher intensities than the

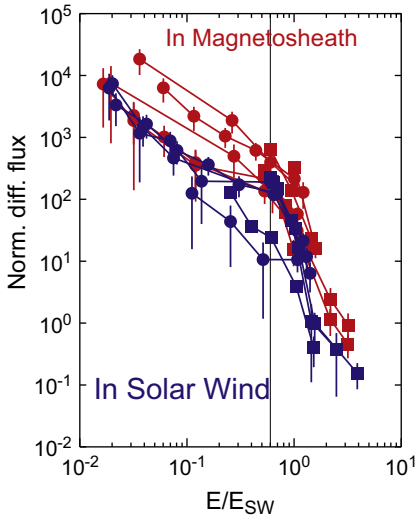

Fig. 7. Same as Fig. 6 but all spectra of the solar wind intervals are shown in blue and those of the magnetosheath intervals in red. A line at $E=0.6\ E_{SW}$ is drawn to guide the eye. The circles refer to IBEX-Lo and the squares refer to IBEX-Hi.

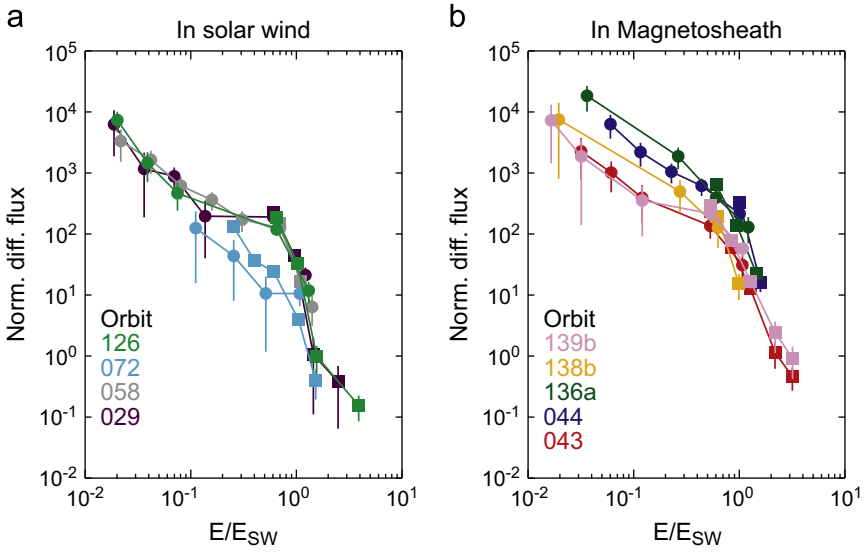

Fig. 6. Normalized spectra when the Moon is in the solar wind (a) and in the magnetosheath and (b). The spectra are color-coded according to orbit number. The circles refer to IBEX-Lo and the squares refer to IBEX-Hi.

other ones. The intensities of magnetosheath intervals also appear to be higher for energies below ~0.6 E_{SW}, even if we disregard the spectrum from orbit 72 (the lowest intensity at ~0.6 E_{SW}). All supersonic solar wind cases fall at the lower edge or below the range of the magnetosheath cases.

3.2. Integrated energy spectra

To perform a more quantitative comparison of the relative intensities of the different energy spectra, we integrate the normalized differential flux over a common range for E/E_{SW}.

Fig. 8 shows each energy spectrum individually. The range of the integration is indicated by the vertical lines. The intensities are interpolated between the data points. The red plot boxes refer to solar wind intervals and the blue ones to the magnetosheath intervals.

We can now compare the total integrated intensity of the different energy spectra.

In Fig. 9, we plot the integrated intensities, which are proportional to the reflection coefficient, as a function of average solar wind energy during the viewing interval. The color coding is the same as for the previous figures. The letter "M" next to the dots refers to magnetosheath intervals and the letter "S" to solar wind intervals. The numbers refer to where the Moon was with respect to the GSE coordinate system. Looking at Fig. 1(a) or (b), the number 1 corresponds to the quarter at the lower right corner, number 2 to the quarter at the upper right, and so on counterclockwise. We chose the solar wind energy for the x-axis because Funsten et al. (2013) reported that the reflection coefficient depends on the solar wind speed. It is about 0.18 for 0.5 keV and decreases to ~0.07 for 2 keV.

Here, we observe a similar dependence between the integrated intensity and the solar wind energy, except that the amount of variation seems much more pronounced here than from the differences in the reflection coefficient quoted above. There is a factor of about 25 between the dark green point (M1) at ~0.75 keV

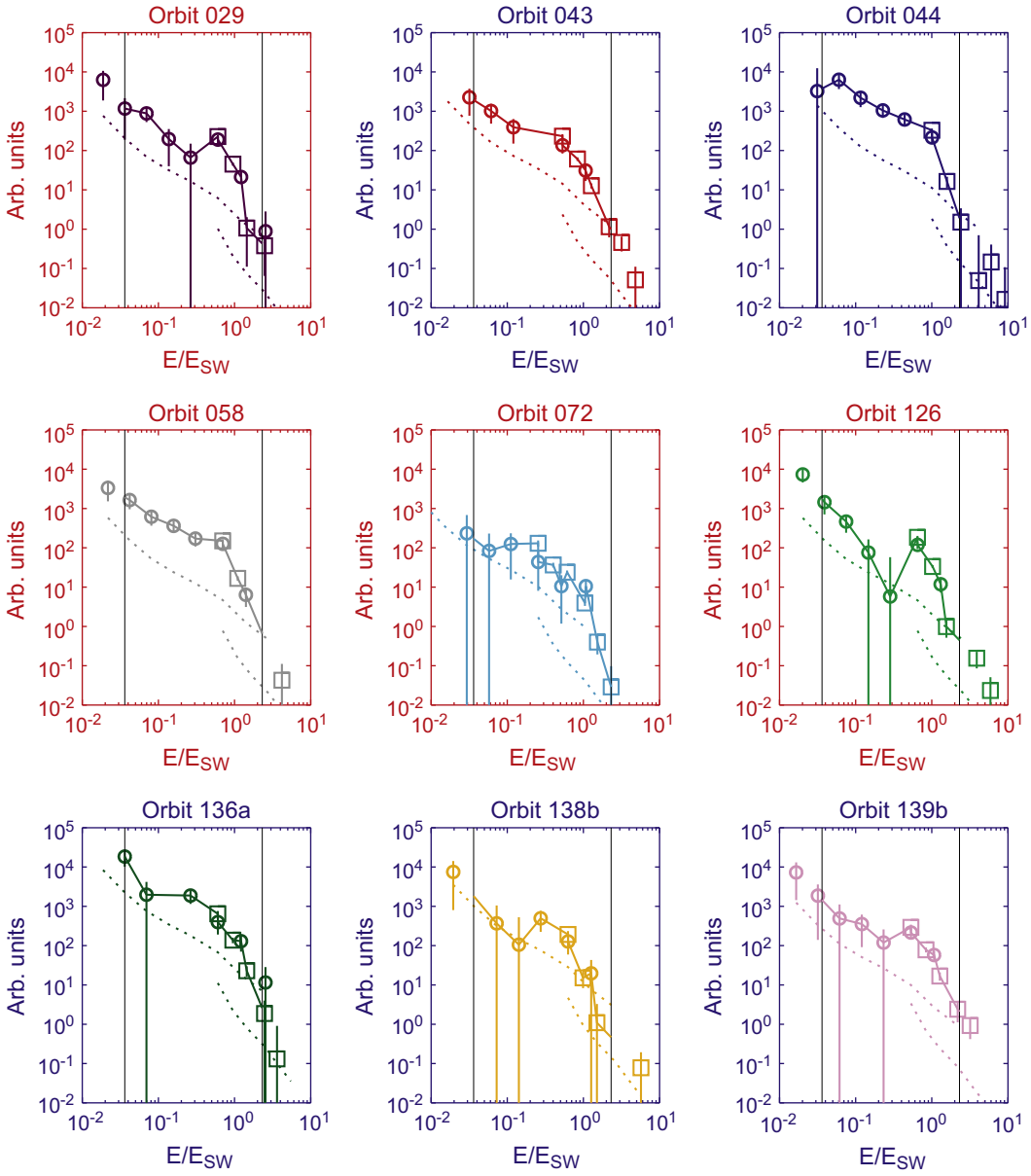

Fig. 8. Energy spectra shown individually for each lunar viewing. The vertical lines show the range of the integration (see text). The red box plots are for solar wind intervals and the blue ones for the magnetosheath intervals. The data points are plotted with the same colors as in Fig. 6. The circles refer to IBEX-Lo and the squares refer to IBEX-Hi.

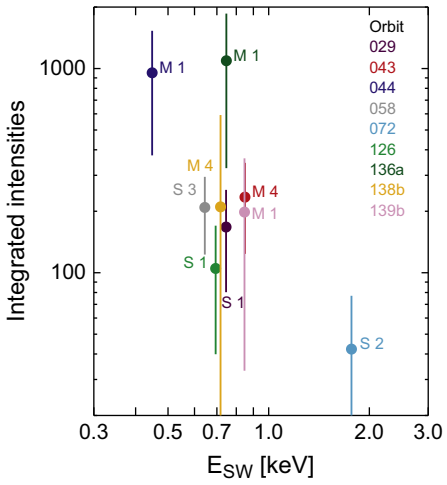

Fig. 9. Integrated intensities of the spectra from Fig. 8 as a function of average solar wind energy during the viewing intervals. The colors are consistent with previous Figures. The letters refer to the location of the Moon for the viewing: M is for magnetosheath and S is for solar wind. The numbers correspond to the quarter in a GSE coordinate system: 1 is for the lower right quarter in Fig. 1(a) or (b) and the number increases for each quarter when going counter-clockwise.

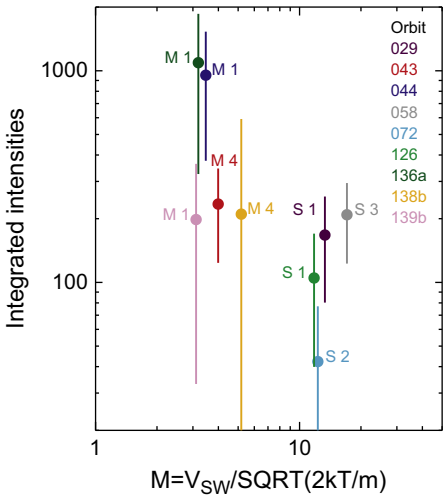

Fig. 10. Same as Fig. 9 but plotted as a function of solar wind Mach number.

and the cyan point (S2) at ~1.8 keV. The dark green point (M1) has a much higher integrated intensity than the large group of points at similar solar wind energies. Moreover, it does not seem to follow the trend outlined by the rest of the data points. If we were to remove this point because of some unaccounted for error, then the trend would be very clear. However, we cannot think of a good reason why this particular point should be removed. It is a point from one of the spectra that has very good statistics.

The integrated intensity of the spectrum of orbit 72 (cyan point S2), which spectrum looked rather below the others (see Figs. 6 and 7), corresponds to the highest solar wind energy—twice the energy of the next point down.

The different integrated intensities do not seem to be ordered by location of the Moon when the viewing occurred. For example, there are three viewings when the Moon was in the magnetosheath ("M") and the first quarter ("1"), but the three data points (blue, dark green, and violet) are not grouped in the same area of the plot. The only trend, which was already identified above, is that the intensities of magnetosheath intervals are higher than those of the solar wind intervals in average.

We mention in the introduction that the Mach number is different in the solar wind and in the magnetosheath because the magnetosheath plasma is "shocked" solar wind at the bow shock. The Mach number is smaller in the magnetosheath, i.e., the solar wind velocity distribution function is broader. Fig. 10 shows the integrated intensities as a function of the solar wind Mach number (proton speed divided by thermal speed). The proton temperature and the solar wind speed are obtained from OMNIWeb and the BASTRUS model. As expected, the magnetosheath lunar viewings have a much lower (below 6) Mach number than the solar wind viewings (above 10). There is no clear trend showing a relationship between the integrated intensities and the Mach number, except that the integrated intensities for $M<6$ are higher in average than for $M>10$.

4. Discussion

Summarizing the main points of our results, we find that:

1. The lunar ENA intensities are higher on average when the Moon is in the magnetosheath than when the Moon is in the solar wind;
2. The energy spectra for all the viewings show a "hump" at about ~0.6 * solar wind energy. Above the "hump" the spectra have a similar form. Below the "hump" the energy spectra for the magnetosheath viewings appear harder (flatter) than for the solar wind viewings. The "hump" is broader for the magnetosheath intervals; it is narrower for the solar wind intervals.

In the following, we discuss ideas regarding these findings.

4.1. Solar wind parameters

The normalization of the energy spectra requires knowledge of a number of solar wind parameters (velocity, density, temperature). Those that are determined by propagating the solar wind from L1 to Earth are probably the most reliable. It is possible, however, that those inferred from the magnetospheric model are inaccurate. If that were true, we do not know which ones would be inaccurate and by how much. It would only be speculative. However, the model output can be used to estimate the uncertainty of the parameters that we obtain by sampling these parameters around the location of the Moon. We use the viewing in orbit 136a as an example. We calculate the average and the standard deviation of the density, the speed, and the flow direction of the plasma in a three-dimensional grid of 1 R_E in every direction around the Moon. At the beginning of the viewing, the standard deviation in this grid is 11% for the density, 1% for the speed, and 0.2° for the flow direction. At the middle of the viewing, it is 6% for the density, 0.3% for the speed, and 0.4° for the flow direction. And at the end of the viewing, it is 6% for the density, 0.6% for the speed, and 0.2° for the flow direction. These uncertainties are much smaller than the differences observed in the integrated intensities.

The ARTEMIS mission (Angelopoulos, 2011) (orbiting around the Moon) could help determining the solar wind parameters in future studies.

4.2. Backscatter locations on the Moon

A separation of the intervals by "quarters" in the GSE coordinate (as shown in Figs. 9 and 10) system may be too coarse to identify systematic differences. Thus, in the following we try to identify the regions on the Moon where the observed ENAs will most likely come from.

Fig. 11 shows on the top a full map of the Moon (from NASA PDS Imaging Node, USGS Astrogeology Research Program) in cylindrical

coordinates and on the bottom the different spectra with the viewing configuration. The longitude (−180° to +180°) is indicated on the top, the latitude range goes from −90° (bottom) to +90° (top), and the equator is horizontal in the middle of the picture.

Because the Moon day is equal to its orbital period around the Earth, the Moon always shows the same face from the Earth point of view. But IBEX "sees" the Moon from a very different vantage point than the Earth because of its high altitude, highly elliptical orbit. The viewings occurred at roughly five groups of locations sketched on the bottom part. The portion of the Moon from where the solar wind can be reflected into IBEX's sensors' apertures is shown in orange, and is simply determined from the solar wind direction and IBEX's location. The other areas on the Moon are either not visible from IBEX or not exposed to the solar wind at the time of the viewings. This orange portion is the same for all the magnetosheath intervals in terms of longitudinal range, but it is different for the solar wind intervals. The ranges in longitude of the orange sectors are delimited by the respective colored vertical lines on the map. For example, the portion where the solar wind reflected from the Moon and potentially detected by IBEX for the viewing during orbit 58 (magenta) corresponds to the interval delimited by the magenta lines on the map. The resulting spectrum is also shown with the same color (on top of the other spectra in gray) on the left. The location of the Moon in orbit 58 is shown next to the number 58 in magenta on the bottom. Other ranges are shown the same way with other colors. The blue range corresponds to all magnetosheath intervals.

Note that two of these areas (orbit 58, magenta; orbit 72, red) are not only limited to the near side of the Moon but also include some areas from the far side. The near and the far sides differ in

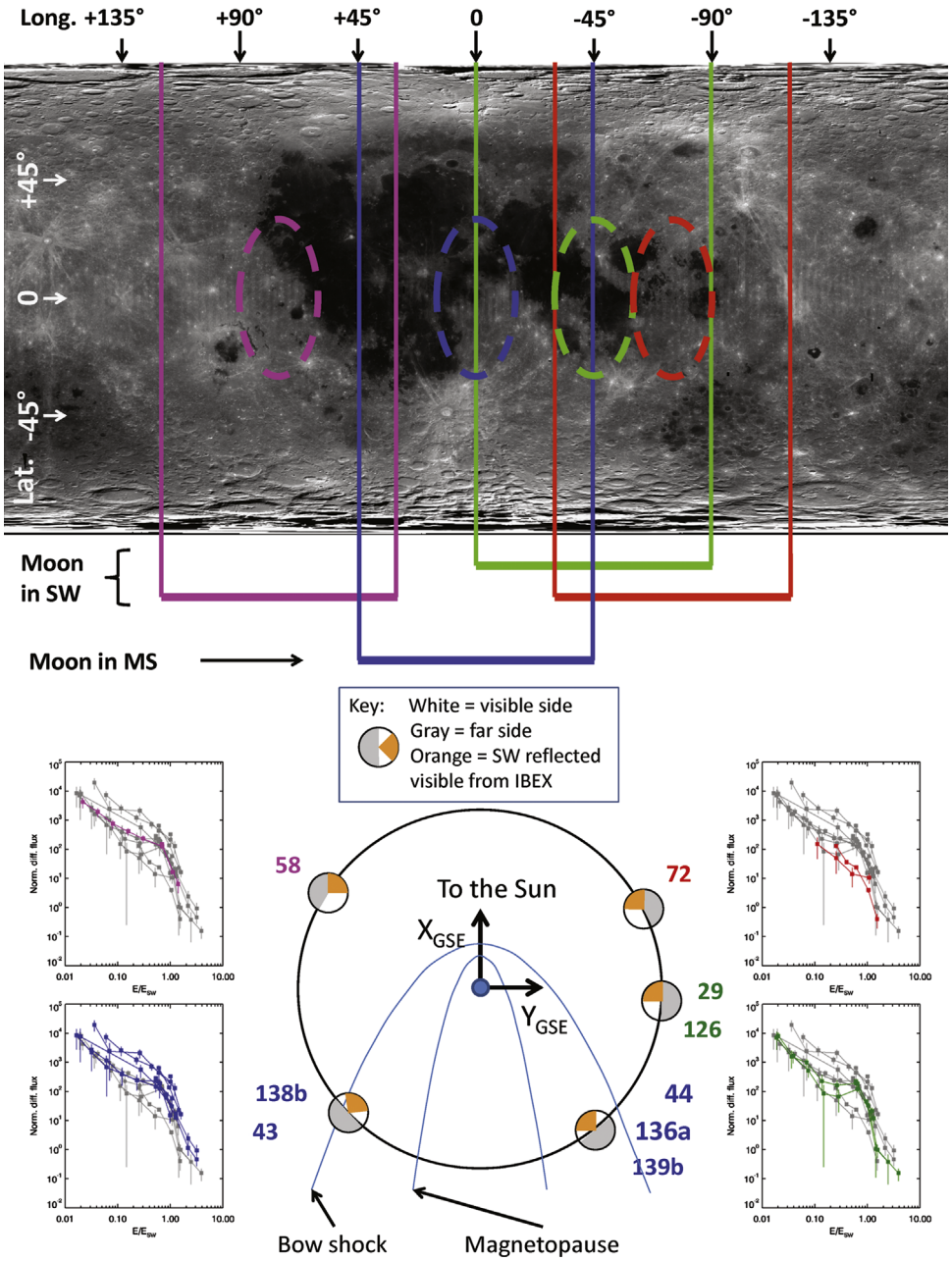

Fig. 11. Full map of the Moon (top) in cylindrical projection showing the near side in the middle (longitude from −90° to +90°) and the far side on the sides. The ranges delimited by the vertical colored lines represent the areas from where the observed ENAs come from on. The colors correspond to the spectra and orbit numbers shown on the bottom. The approximate location of the Moon in a GSE coordinate system is illustrated.

composition and also in terrain. The far side is more highland–like, whereas the near side contains a lot of mare. We can reduce the size of the ranges because even though ENAs from these ranges can reach IBEX, not all the area reflects the same amount of solar wind towards IBEX. Using the results from Schaufelberger et al. (2011), we determined that the dashed ovals were the areas that should produce the highest intensities of ENAs measurable from IBEX's point of view. In other words, we can expect that most of the intensities are due to ENAs that were reflected from these areas.

The green oval (for orbits 29 and 126) covers almost entirely mare while the red oval (for orbit 72; lowest integrated intensity) and the magenta oval (for orbit 58) cover mostly highlands. The blue oval (for all magnetosheath viewings; highest integrated intensities) covers about half mare and half highlands. There does not seem to be a systematic pattern based on the topography that can explain the differences between the intensities observed.

4.3. Effects of the Mach number

The plasma in the magnetosheath has a lower Mach number than outside the magnetosphere in the solar wind. Thus, the velocity distribution function (VDF) in the magnetosheath is broader than that in the solar wind. In other words, the angular distribution of the solar wind impinging on the lunar surface is broader in the magnetosheath than it is in the solar wind. We examine the effects that this broader distribution has on the backscattered ENAs at two different scales: a macroscopic scale where the Moon is viewed as a sphere and a microscopic scale where we focus on the grains that backscatter solar wind.

On a macroscopic scale, the area illuminated by the solar wind and visible from IBEX is larger when the Mach number is lower (the angular distribution of impinging solar wind is larger). For our observations, we expect an increase of about 3% in ENA flux. Although this is not sufficient to explain a factor of 10 or more, it contributes to the differences observed.

On a microscopic level, we have to take into account the structure of the regolith. It is composed of small grains and rocks with a very rough surface. Fig. 12 illustrates grains and backscattered ENAs and shows the effect of surface structure for two cases where the magnetosheath plasma has a low *M* and the solar wind has a high *M*. In the case of a high *M* number the angular distribution of the impinging solar wind is narrow. The area that the solar wind reaches is almost like a projection. In the case of the magnetosheath plasma (low *M*), the angular distribution is broader. As a consequence, some areas that the cold solar wind could not reach are now illuminated by this hotter wind providing additional surface area for backscattering solar wind. Hence, the total surface illuminated by the hot solar wind is larger and there are more backscattered ENAs that can reach IBEX.

While both mechanisms contribute to an increase in the backscatter ENA flux–at microscopic and macroscopic scales–are analogous because they invoke the area where backscattered ENAs are created, they differ in the sense that the mechanism at a microscopic scale would not exist for a smooth surface. They both, however, contribute to an increase of the backscattered ENA flux.

Another consequence of differences in the *M* number is that the velocity distribution function (VDF) is also different. A higher M number corresponds to a narrower VDF and a lower M number corresponds to a wider VDF. Thus, there is more low-velocity (or speed) solar wind for a lower M number than for a higher M number. Since the ENA albedo is higher for lower speeds, it is possible that, for a constant solar wind flux, the wider VDF favors backscattering compared to the narrower VDF.

The shape of the "hump" in the energy spectra shows a hint of the effects of the solar wind distribution functions. The "hump" is narrow for solar wind intervals–narrow VDF–and it is broad for magnetosheath intervals–wide VDF.

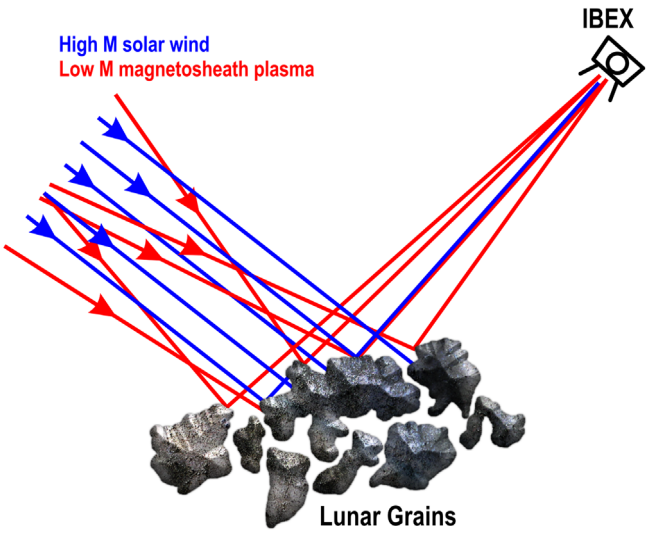

Fig. 12. High Mach number (cold) solar wind in blue has a narrower angular distribution compared with low Mach number (hot) solar wind. Hot solar wind has access to more surface area that can backscatter ENAs into IBEX's aperture.

At this point it is not clear if the differences in the *M* number that are described above can explain the large differences observed in the integrated intensities. Nevertheless, they all point towards the same conclusion: a lower M number, as observed in the magnetosheath, results in higher backscattered ENA intensities. From these observations and previous reports, a very likely situation is that both the impinging plasma speed and Mach number play a role in determining the intensities. More observations of this type will show if a relationship between the Mach number and the ENA intensities exists and, if so, will help quantifying that relationship.

5. Conclusion

IBEX measures ENAs from solar wind reflected off the surface of the Moon. We selected nine intervals during which both IBEX-Lo and -Hi sensors observed these lunar ENAs. For five of them the Moon was inside the magnetosheath, and for the remaining four the Moon was in the solar wind. We showed for the first time combined IBEX-Lo and -Hi energy spectra of the lunar ENAs. The spectra are very consistent above ~0.6*solar wind energy, but there are large differences ($>$ factor of 10) between them at lower energies. We calculated the total integrated intensities and compared them for all the viewings. On average, the integrated intensities are higher when the Moon is in the magnetosheath than when it is in the solar wind. The energy spectra have the form of a power law with a "hump" at ~0.6* solar wind energy. The shape of the "hump" is narrower for solar wind viewings than for magnetosheath viewings.

By mapping the regions on the Moon where most of the ENAs are coming from, we did not find any systematic topographical pattern that could explain the differences between the spectra. A more likely scenario is based on the differences in the Mach number. Solar wind with a smaller Mach number can reach more of the lunar surface and naturally produces more backscattered ENAs. It is difficult to estimate the increase factor at this point. We expect that with more lunar ENA observations by IBEX, we will be able to shed more light on this issue. Thus, we have shown the first IBEX observations of ENAs from the Moon inside the

magnetosheath which reveals the higher neutralization and reflection of plasma potentially due its reduced Mach number.

Acknowledgments

We thank all the outstanding men and women that have made IBEX such a successful mission.

We acknowledge the use of ACE and Wind solar wind data, provided through the OMNIWeb Plus data at Goddard Space Flight Center through their public through their public interface. Simulation results have been provided by the Community Coordinated Modeling Center at Goddard Space Flight Center through their public Runs on Request system (http://ccmc.gsfc.nasa.gov). The CCMC is a multi-agency partnership between NASA, AFMC, AFOSR, AFRL, AFWA, NOAA, NSF and ONR. The BATSRUS Model was developed by the Dr. Tamas Gombosi et al. at the Center for Space Environment Modeling, University of Michigan. We also acknowledge the use of a Clementine basemap V2 map obtained from NASA PDS Imaging Node, USGS Astrogeology Research Program. D.F.R.M. and P.W. acknowledge the financial support by the Swiss national Science Foundation.

References

Allegrini, F., Crew, G.B., Demkee, D., Funsten, H.O., McComas, D.J., Randol, B., Rodriguez, B., Schwadron, N.A., Valek, P., Weidner, S, 2009. The IBEX background monitor. Space Science Review 146, 105–115, http://dx.doi.org/10.1007/s11214-008-9439-8.

Angelopoulos, V., 2011. The ARTEMIS mission. Space Science Review 165, 3–25, http://dx.doi.org/10.1007/s11214-010-9687-2.

Barabash, S., Bhardwaj, A., Wieser, M., Sridharan, R., Kurian, T., Varier, S., Vijayakumar, E., Abhirami, V., Raghavendra, K.V., Mohankumar, S.V., Dhanya, M.B., Thampi, S., Kazushi, A., Andersson, H., Yoshifumi, F., Holmström, M., Lundin, R., Svensson, J., Karlsson, S., Piazza, D., Wurz, P., 2009. Investigation of the solar wind—Moon interaction onboard Chandrayaan-1 mission with the SARA Experiment. Current Science 96, 526–532.

Bhardwaj, A., Barabash, S., Futaana, Y., Kazama, Y., Asamura, K., Sridharan, R., Holmström, M., Wurz, P., Lundin, R., 2005. Low energy neutral atom imaging on the Moon with the SARA instrument aboard Chandrayaan-1 mission. Journey Earth System Science 114 (6), 749–760.

Funsten, H.O., McComas, D.J., Barraclough, B.L., 1993. Ultrathin foils used for low-energy neutral atom imaging of the terrestrial magnetosphere. Optical Engineering 32 (12), 3090.

Funsten, H.O., Allegrini, F., Bochsler, P., Dunn, G., Ellis, S., Everett, D., Fagan, M.J., Fuselier, S.A., Granoff, M., Gruntman, M., Guthrie, A.A., Hanley, J., Harper, R.W., Heirtzler, D., Janzen, P., Kihara, K.H., King, B., Kucharek, H., Manzo, M.P., Maple, M., Mashburn, K., McComas, D.J., Moebius, E., Nolin, J., Piazza, D., Pope, S., Reisenfeld, D.B., Rodriguez, B., Roelof, E.C., Saul, L., Turco, S., Valek, P., Weidner, S., Wurz, P., Zaffke, S., 2009. The Interstellar Boundary Explorer High Energy (IBEX-Hi) neutral atom imager. Space Science Review 146, 75–103, http://dx.doi.org/10.1007/s11214-009-9504-y.

Funsten, H.O., Allegrini, F., Bochsler, P.A., Fuselier, S.A., Gruntman, M., Henderson, K., Janzen, P.H., Johnson, R.E., Larsen, B.A., Lawrence, D.J., McComas, D.J., Möbius, E., Reisenfeld, D.B., Rodriguez, D., Schwadron, N.A., Wurz, P., 2013. Reflection of solar wind hydrogen from the lunar surface. Journal of Geophysical Research: Planets 118, 292, http://dx.doi.org/10.1002/jgre.20055.

Fuselier, S.A., Bochsler, P., Chornay, D., Clark, G., Crew, G.B., Dunn, G., Ellis, S., Friedmann, T., Funsten, H.O., Ghielmetti, A.G., Googins, J., Granoff, M.S., Hamilton, J.W., Hanley, J., Heirtzler, D., Hertzberg, E., Isaac, D., King, B., Knauss, U., Kucharek, H., Kudirka, F., Livi, S., Lobell, J., Longworth, S., Mashburn, K., McComas, D.J., Möbius, E., Moore, A.S., Moore, T.E., Nemanich, R.J., Nolin, J., O'Neal, M., Piazza, D., Peterson, L., Pope, S.E., Rosmarynowski, P., Saul, L.A., Scherrer, J.R., Scheer, J.A., Schlemm, C., Schwadron, N.A., Tillier, C., Turco, S., Tyler, J., Vosbury, M., Wieser, M., Wurz, P., Zaffke, S., 2009. The IBEX-Lo Sensor. Space Science Review 146, 117–147, http://dx.doi.org/10.1007/s11214-009-9495-8.

Fuselier, S.A., Funsten, H.O., Heirtzler, D., Janzen, P., Kucharek, H., McComas, D.J., Moebius, E., Moore, T.E., Petrinec, S.M., Reisenfeld, D.B., Schwadron, N.A., Trattner, K.J., Wurz, P., 2010. Energetic neutral atoms from the Earth's subsolar magnetopause. Geophysical Research Letters 37, L13101, http://dx.doi.org/10.1029/2010GL044140.

Fuselier, S.A., Allegrini, F., Bzowski, M., Funsten, H., Ghielmetti, A., Gloeckler, G., Heirtzler, D., Janzen, P., Kubiak, M., Kucharek, H., McComas, D.J., Moebius, E., Moore, T., Petrinec, S., Quinn, M., Reisenfeld, D., Saul, L., Scheer, J., Schwadron, N., Trattner, K., Vanderspek, R., Wurz, P., 2012. Heliospheric neutral atom spectra between 0.01 and 6 keV from IBEX. Astrophysical Journal 754, 14.

Futaana, Y., Barabash, S., Wieser, M., Holmström, M., Lue, C., Wurz, P., Schaufelberger, A., Bhardwaj, A., Dhanya, M.B., Asamura, K., 2012. Empirical energy spectra of neutralized solar wind protons from the lunar regolith. Journal of Geophysical Research 117, E05005.

McComas, D.J., Allegrini, F., Bochsler, P., Bzowski, M., Collier, M., Fahr, H., Fichtner, H., Funsten, H., Fuselier, S., Gloeckler, G., Gruntman, M., Izmodenov, V., Knappenberger, P., Lee, M., Livi, S., Mitchell, D., Möbius, E., Moore, T., Pope, S., Reisenfeld, D., Roelof, E., Scherrer, J., Schwadron, N., Tyler, R., Wieser, M., Witte, M., Wurz, P., Zank, G., 2009a. IBEX—the interstellar boundary explorer. Space Science Review 146, 11–33.

McComas, D.J., Allegrini, F., Bochsler, P., Frisch, P., Funsten, H.O., Gruntman, M., Janzen, P.H., Kucharek, H., Möbius, E., Reisenfeld, D.B., Schwadron, N.A., 2009b. Lunar backscatter and neutralization of the solar wind: first observations of neutral atoms from the Moon. Journal of Geophysical Research 36, L12104.

McComas, D.J., Carrico, J.P., Hautamaki, B., Intelisano, M., Lebois, R., Loucks, M., Policastri, L., Reno, M., Scherrer, J., Schwadron, N.A., Tapley, M., Tyler, R., 2011a. A new class of long-term stable lunar resonance orbits: space weather applications and the interstellar boundary explorer. Space Weather 9, S11002, http://dx.doi.org/10.1029/2011SW000704.

McComas, D.J., Dayeh, M.A., Funsten, H.O., Fuselier, S.A., Goldstein, J., Jahn, J.-M., Janzen, P., Mitchell, D.G., Petrinec, S.M., Reisenfeld, D.B., Schwadron, N.A., 2011b. First IBEX observations of the terrestrial plasma sheet and a possible disconnection event. Journal of Geophysical Research 116, A02211, http://dx.doi.org/10.1029/2010JA016138.

McComas, D.J., Buzulukova, N., Connors, M.G., Dayeh, M.A., Goldstein, J., Funsten, H. O., Fuselier, S., Schwadron, N.A., Valek, P., 2012. TWINS and IBEX ENA imaging of the 5 April 2010 substorm. Journal of Geophysical Research 117, A03225, http://dx.doi.org/10.1029/2011JA017273.

Petrinec, S.M., Dayeh, M.A., Funsten, H.O., Fuselier, S.A., Heirtzler, D., Janzen, P., Kucharek, H., McComas, D.J., Möbius, E., Moore, T.E., Reisenfeld, D.B., Schwadron, N.A., Trattner, K.J., Wurz, P., 2011. Neutral atom imaging of the magnetospheric cusps. Journal of Geophysical Research 116, A07203, http://dx.doi.org/10.1029/2010JA016357.

Rodríguez, M., Saul, D.F., Wurz, L., Fuselier, P., Funsten, S.A., McComas, H.O., Möbius, E., D.J., 2012. IBEX-Lo observations of energetic neutral hydrogen atoms originating from the lunar surface. Planetary and Space Science 60, 297–303.

Saul, L., Wurz, P., Vorburger, A., Rodríguez, M.D.F., Fuselier, S.A., McComas, D.J., Möbius, E., Barabash, S., Funsten, H.O., Janzen, P., 2013. Solar wind reflection from the lunar surface: the view from far and near. Planetary and Space Science, in press.

Schaufelberger, A., Wurz, P., Barabash, S., Wieser, M., Futaana, Y., Holmström, M., Bhardwaj, A., Dhanya, M.B., Sridharan, R., Asamura, K., 2011. Scattering function for energetic neutral hydrogen atoms off the lunar surface. Geophysical Research Letters 38, L22202.

Wieser, M., Barabash, S., Futaana, Y., Holmström, M., Bhardwaj, A., Sridharan, R., Dhanya, M.B., Wurz, P., Schaufelberger, A., Asamura, K., 2009. Extremely high reflection of solar wind protons as neutral hydrogen atoms from regolith in space. Planetary and Space Science 57, 2132.

Scheer, J.A., Wieser, M., Wurz, P., Bochsler, P., Hertzberg, E., Fuselier, S.A., Koeck, F.A., Nemanich, R.J., Schleberger, M., 2006. Conversion surfaces for neutral particle imaging detectors. Advances in Space Research 38, 664.

Kazama, Y., Barabash, S., Wieser, M., Asamura, K., Wurz, P., 2007. Development of an LENA instrument for planetary missions by numerical simulations. Planetary and Space Science 55, 1518–1529, http://dx.doi.org/10.1016/j.pss.2006.11.027.

Wurz, P., Scheer, J., Wieser, M., 2006. Particle scattering off surfaces: application in space science. e-Journal Surface Science Nanotechnology 4, 394–400.

Wurz, P., 2000. Detection of energetic neutral particles. In: Scherer, K., Fichtner, H., Marsch, E. (Eds.), The Outer Heliosphere: Beyond the Planets. Copernicus Gesellschaft e.V., Katlenburg-Lindau, Germany, pp. 251–288.